A Dye-Sensitized Photoelectrochemical Tandem Cell for Light Driven Hydrogen Production from Water

Benjamin D. Sherman, Matthew V. Sheridan, Kyung-Ryang Wee,[†] Seth L. Marquard, Degao Wang, Leila Alibabaei, Dennis L. Ashford, and Thomas J. Meyer*

Department of Chemistry, University of North Carolina at Chapel Hill, Chapel Hill, North Carolina 27599, United States

S Supporting Information

ABSTRACT: Tandem junction photoelectrochemical water-splitting devices, whereby two light absorbing electrodes targeting separate portions of the solar spectrum generate the voltage required to convert water to oxygen and hydrogen, enable much higher possible efficiencies than single absorber systems. We report here on the development of a tandem system consisting of a dye-sensitized photoelectrochemical cell (DSPEC) wired in series with a dye-sensitized solar cell (DSC). The DSPEC photoanode incorporates a tris(bipyridine)ruthenium(II)-type chromophore and molecular ruthenium based water oxidation catalyst. The DSPEC was tested with two more-red absorbing DSC variations, one utilizing N719 dye with an I_3^-/I^- redox mediator solution and the other D35 dye with a tris(bipyridine)cobalt ($[Co(bpy)_3]^{3+/2+}$) based mediator. The tandem configuration consisting of the DSPEC and D35/$[Co(bpy)_3]^{3+/2+}$ based DSC gave the best overall performance and demonstrated the production of H_2 from H_2O with the only energy input from simulated solar illumination.
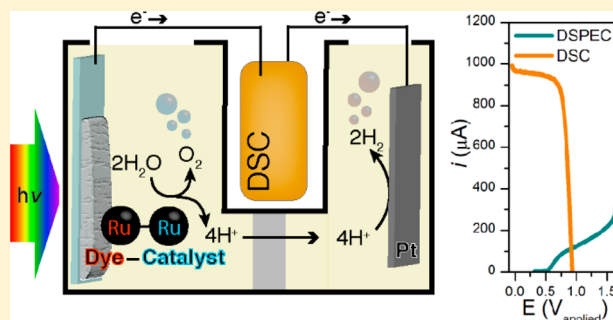
INTRODUCTION

Human beings have come to dominate nearly all ecosystems on the planet.[1,2] The scale and scope of human activity in turn has a profound impact on planet level systems, from the energy balance of the biosphere[3] to geochemical cycles such as that of carbon, nitrogen, and water.[1,4] Reliance on the burning of fossil fuels as the primary energy resource, in particular, represents a major driver of anthropogenic changes to the planet.[2,3]

By establishing technologies for harnessing solar energy to convert abundant precursors such as H_2O and CO_2 to fuels, the field of Artificial Photosynthesis seeks to augment mankind's reliance on sequestered carbon sources.[5−7] Artificial photosynthesis derives inspiration from the process of oxygenic photosynthesis which uses sunlight to convert water and CO_2 to reduced carbon compounds.[8] An essential aspect of this process involves the absorption of two photons per electron that traverses Photosystem II and Photosystem I. Thermodynamic accounting of the possible efficiency for converting solar energy to a fuel shows a tandem junction approach such as this is imperative to achieving the highest possible solar energy conversion efficiencies.[9−11]

Several multijunction photoelectrochemical solar cell configurations have appeared in the literature including semiconductor photovoltaic (PV) based systems,[12,13] direct band gap absorbing semiconductor based photoelectrochemical cell−dye-sensitized solar cell (PEC−DSC) systems,[14−16] and fully dye-sensitized photoelectrochemical cell-based configurations (DSPEC). Of the latter, two configurations have been described consisting of either a dye-sensitized photoanode connected to a dye-sensitized photocathode[17] (tandem DSPEC) or two photoanode based cells wired in series (DSPEC−DSC).[18] The tandem cell described here uses the second type of configuration, employing an n-type dye-sensitized photoanode in both the DSPEC and DSC component cells. This type of configuration was pursued to avoid the need for a photocathode based on a p-type semiconductor such as NiO or CuO which typically demonstrates inferior photochemical performance in DSCs[19] as compared to n-type oxides (usually TiO_2 or SnO_2).[20]

This study outlines, for the first time, a tandem dye-sensitized photoelectrochemical system using n-type photoanodes that can perform the net conversion of water to O_2 and H_2 with the only energy input from light. The tandem cell studied consists of a DSPEC wired in series with a DSC, with each component cell consisting of a photoanode and dark cathode. In this configuration, the photoanode of the DSPEC connects to the cathode of the DSC and the photoanode of the DSC connects to the cathode of the DSPEC. A Nafion membrane separates the anodic and cathodic sides of the DSPEC to enable charge balance across the DSPEC while preventing O_2 or H_2 product crossover.

Similar tandem configurations specifically using a DSC to supply the needed voltage bias to sustain overall water splitting have appeared in the literature using PEC photoanodes incorporating hematite,[14,21] tungsten oxide (WO_3),[14,22] or bismuth vanadate ($BiVO_4$)[16] light absorbing layers. Recently a

DSPEC—DSC tandem cell has been reported, with the photochemical production of H_2 coinciding with the consumption of a sacrificial donor (hydroquinone).[18] Here we demonstrate the production of H_2 with water as the electron source using a SnO_2/TiO_2 core—shell photoanode with an electro-assembled surface layer containing a $[RuP]^{2+}$ ([ruthenium(5,5′-divinyl-2,2′-bipyridine)$_2$(2,2′-bipyridine-4,4′-diylbis(phosphonic acid))]$^{2+}$) based chromophore and [Ru(bda)(isoq)$_2$] (bda = 2,2′-bipyridine-6,6′-dicarboxylic acid; isoQ = 5-(pen-4-en-1-yloxy)isoquinoline) water oxidation catalyst.

■ EXPERIMENTAL SECTION

General. All chemicals were purchased from Sigma-Aldrich or Alpha Aesar and used as received unless otherwise noted. The fluorine doped tin oxide (FTO) electrodes (TEC 15) were purchased from Hartford glass (Hartford, IN). Nafion membrane was purchased from FuelCellsEtc (College Station, TX). Hydrogen measurements were performed using an electrochemical sensor with an analyte specific response (Unisense, Denmark). The production of oxygen was verified using a collector—generator dual electrode technique, and a detailed description of this method is reported elsewhere.[23] A Thor Laboratories HPLC-30-04 plasma light source was used to provide 1 sun (100 mW cm^{-2}) white light illumination, and a 400 nm long-pass filter was placed in front of the samples to avoid any direct band gap illumination of TiO_2. A CH Instruments 601D potentiostat was used for the electro-assembly procedure, and a CH Instruments 760E bipotentiostat was used for the photochemical measurements.

Synthesis. All manipulations were carried out under an inert atmosphere unless otherwise noted. All ^1H NMR spectra were obtained on a Bruker Advance spectrometer at 400 MHz and recorded relative to residual protio solvent. All other reagents and solvents were obtained from commercial sources and used without further purification. The synthetic procedure for preparing the [ruthenium(5,5′-divinyl-2,2′-bipyridine)$_2$(2,2′-bipyridine-4,4′-diylbis(phosphonic acid))]$^{2+}$ ([RuP]$^{2+}$) chromophore appears in an earlier publication.[24] The [ruthenium(2,2′-bipyridine-6,6′-dicarboxylic acid)(dimethyl sulfoxide)$_2$] ([Ru(bda)(DMSO)$_2$]) precursor used for preparing the [Ru(bda)(isoq)$_2$] catalyst was prepared according to literature methods.[25] Synthetic procedures for preparing the D35[26] dye and [Co(bpy)$_3$]$^{3+/2+}$ mediator[27] can also be found in previous publications.

Synthesis of 5-(Pent-4-en-1-yloxy)isoquinoline. A 100 mL round-bottom flask was charged with 5-hydroxyisoquinoline (687 mg, 4.73 mmol), 5-bromo-1-pentene (697 mg, 4.67 mmol), and potassium carbonate (1.34 g, 9.70 mmol). The flask was equipped with a reflux condenser and flushed with nitrogen, and then dry acetonitrile (30 mL) was introduced via syringe. The resulting suspension was heated at 85 °C for 72 h. The resulting dark red suspension was then cooled to room temperature, and the solvent was removed by rotary evaporation. The crude material was purified by silica gel chromatography using 25% ethyl acetate/hexanes to elute the colorless product ($R_f \approx 0.3$). The product containing fractions were combined, and the solvent was removed by rotary evaporation affording 222 mg (22%) of the product as a pale yellow oil. ^1H NMR (400 MHz, CDCl$_3$): δ 9.20 (s, 1H), 8.53 (d, J = 6.0 Hz, 1H), 8.03 (d, J = 6.0 Hz, 1H), 7.55−7.49 (m, 2H), 7.0 (dd, J = 1.2, 7.6 Hz, 1H), 5.90 (ddt, J = 6.5, 10.4, 17.2 Hz, 1H), 5.09 (ddt, J = 1.6, 3.2, 17.2 Hz, 1H), 5.03 (ddt, J = 1.2, 2.8, 10.0 Hz, 1H), 4.16 (t, J = 8.0 Hz, 2H), 2.35 (q, J = 7.1 Hz, 2H), 2.04 (pent, J = 6.9 Hz, 2H).

Synthesis of [Ruthenium(2,2′-bipyridine-6,6′-dicarboxylic acid)(5-(pent-4-en-1-yloxy)isoquinoline)$_2$]. An oven-dried 100 mL three-necked round-bottom flask was charged with [Ru(bda)(DMSO)$_2$] (106 mg, 0.212 mmol) and 5-(pent-4-en-1-yloxy)isoquinoline (97 mg, 0.455 mmol). The flask was equipped with a reflux condenser and flushed with nitrogen. Dry methanol (30 mL) was introduced via syringe, and the resulting suspension was sparged with nitrogen. After 15 min the suspension was heated at 85 °C for 5 h resulting in a dark red solution. The reaction mixture was cooled to room temperature and

then filtered through a 0.22 μm syringe filter to remove any unreacted starting material. The solvent was evaporated in vacuo affording a dark red residue. The residue was treated with diethyl ether to precipitate the product as a dark red powder which was filtered and washed with 20 mL of fresh diethyl ether. The collected solid was dried in vacuo affording 153 mg (95%) of the product as a fine red powder. After isolation the product was stored under an inert atmosphere. ^1H NMR (400 MHz, MeOD): δ 8.70 (d, J = 8.0 Hz, 2H), 8.62 (s, 2H), 8.05 (d, J = 7.6 Hz, 2H), 7.95 (t, J = 8.0 Hz, 2H), 7.83 (d, J = 6.8 Hz, 2H), 7.61 (d, J = 6.8 Hz, 2H), 7.54 (t, J = 8.0 Hz, 2H), 7.39 (d, J = 8.0 Hz, 2H), 7.14 (d, J = 8.0 Hz, 2H), 5.86 (ddt, J = 6.5, 10.4, 17.2 Hz, 2H), 5.02 (ddt, J = 1.6, 3.2, 17.2 Hz, 2H partially obscured by the water signal), 4.95 (ddt, 2H, partially obscured by the water signal), 4.13 (t, J = 6.2 Hz, 4H), 2.27 (q, J = 6.6 Hz, 4H), 1.95 (pent, J = 6.7 Hz, 4H).

Preparation of the DSPEC Photoanode. SnO_2/TiO_2 core—shell electrodes were prepared as previously described.[28] Briefly, the prepared SnO_2 paste was doctor bladed onto FTO electrodes and sintered at 450 °C for 45 min. This resulted in 6−8 μm thick mesoporous electrodes. To form the TiO_2 shell, the electrodes underwent 50 cycles of Ti atomic layer deposition (ALD) (Cambridge instruments) using a tetra(dimethlyamido) titanium (TDMAT) precursor.[29] The procedure followed for forming the TiO_2 layer via ALD typically formed ~2 nm films. The SnO_2/TiO_2 electrodes were sintered at 450 °C for 30 min following the ALD treatment.

A similar procedure as described previously was followed for preparing the electro-assembled surfaces.[28] To start, the SnO_2/TiO_2 electrodes were soaked in a solution of the [Ru(5,5′-divinyl-2,2′-bipyridine)$_2$(2,2′-bipyridine-4,4′-diylbis(phosphonic acid))]$^{2+}$ dye in methanol (200 μM) to form a monolayer bound to the surface via the phosphonate anchoring group. The electrodes then underwent 5 cycles of ALD using the same TDMAT precursor and same cycle parameters as used in forming the TiO_2 shell layer.[29] The as-prepared SnO_2/TiO_2|RuP(TiO_2) electrodes then underwent electrochemical deposition of the [Ru(bda)(isoq)$_2$] from acetonitrile solution with 0.1 M tetrabutyl-ammonium hexafluorophosphate supporting electrolyte. The electrochemical procedure for forming the assembly involved 200 potential step cycles consisting of a 1 s hold at −1.8 V vs Ag$^+$/Ag followed by a 5 s hold at −0.5 V vs Ag$^+$/Ag.[28] The deposition of the catalyst was verified by comparison of cyclic voltammograms (CVs) taken before and after the deposition procedure (Figure S1).

DSC Preparation. To assemble the DSC, FTO substrates were cleaned with acetone in an ultrasonic bath for 30 min, followed by rinsing with water and ethanol. Mesoporous TiO_2 films (0.28 cm^2 active area) were prepared by screen printing colloidal TiO_2 paste (Dyesol DSL 18NR-T) and drying at 125 °C between deposition steps. A TiO_2 scattering layer (Dyesol WER2-O) was deposited on top of the mesoporous TiO_2 film. The electrodes (total thickness of 12 μm) were then heated to 500 °C with a programmed temperature ramping as described elsewhere.[30] Before use, a final heating process was performed at 500 °C for 30 min, and after cooling down, the electrodes were immersed in 0.2 mM D35 in ethanol or 0.3 mM N719 in a mixture of acetonitrile and *tert*-butanol (1:1 = v/v) for 16 h.

Sandwich DSCs were assembled with Pt coated FTO glass as the counter electrode using Surlyn film (Solaronix, 25 μm) as a spacer. Electrolyte was injected by vacuum backfilling through a port drilled through the FTO−Pt counter, and the hole was covered by Surlyn film and a cover glass prior to use. The DSC incorporating dye D35 contained electrolyte composed of 0.8 M 4-*tert*-butylpyridine, 0.1 M LiClO$_4$, 0.2 M [Co(bpy)$_3$]$^{2+}$, and 0.066 M [Co(bpy)$_3$]$^{3+}$ in acetonitrile following a protocol from literature.[27] The DSC containing N719 dye used an I$_3^-$/I$^-$ electrolyte containing 0.03 M I$_2$, 0.05 M LiI, 1.0 M 1,3-dimethylimidazolium iodide (Solaronix), 0.1 M guanidinium thiocyanate, and 0.5 M 4-*tert*-butylpyridine in acetonitrile/valeronitrile (85:15 = v/v).

Tandem Photoelectrochemical Measurements. The DSPEC and DSC components of the tandem cell were assembled separately, positioned in parallel relative to the light source (i.e., light first traverses the DSPEC photoanode, then the transmitted light contacts the DSC photoanode such that the total photon flux through the two photoelectrodes sums to AM 1.5 illumination), and wired in a series

circuit. To monitor the current during operation of the tandem cell, the working lead of a potentiostat was connected to the photoanode of the DSPEC and the counter and reference leads were connected to the cathode of the DSC; the current was measured over time with a 0 V applied bias. Alternatively, the potentiostat leads were connected across the other leg of the circuit (between the photoanode of the DSC and cathode of the DSPEC), and this gave the same current response, as expected from a series circuit. An electrochemical sensor (Unisense) operating independently was placed in the sealed head space of the cathodic chamber of the DSPEC to measure photochemically produced H_2.

■ RESULTS AND DISCUSSION

Water Oxidizing Photoanode. The use of electro-polymerization to form redox active films on conducting surfaces has proven an effective method for immobilizing molecular complexes for heterogeneous catalysis.[31−33] Previously, we used this approach to form photoactive chromophore−catalyst films on metal oxide semiconductor surfaces for performing light driven water oxidation.[24,28] This work demonstrated that a $[RuP]^{2+}-[Ru(bda)\ (picoline)_2]$ electro-assembly formed on a SnO_2/TiO_2 core−shell electrode can execute light-driven water oxidation at an applied bias of 0.4 V vs SCE with a faradaic efficiency of 22% in pH 7 media.[28] As described in that study as well as in other work,[34−36] the use of a SnO_2 core with a TiO_2 shell is important for preventing recombination to oxidized surface species after light driven charge separation. While this was an encouraging result, this system did show a gradual decay in the photocurrent over several minutes coinciding with a decrease in the faradaic efficiency for O_2 generation. The observed instability of the surface likely resulted from gradual desorption of surface film components, oxidative decomposition of the photo-oxidized Ru(III) form of the chromophore, or a combination of these factors.[37−40]

This report explores several strategies to improve the stability and long-term functionality of the electro-assembled surface. To avoid any surface desorption of the film, atomic layer deposition (ALD) was used to deposit a coating of TiO_2 on the electrode surface after soaking the electrode in a methanol solution containing 200 μM of $[RuP]^{2+}$. This strategy has proven to be an effective method for stabilizing the surface adsorption of the phosphonate anchoring group, even at elevated pH.[29,41] After ALD treatment of the chromophore-bound surface, electro-assembly of the $[Ru(bda)(isoq)_2]$ catalyst followed a previously reported protocol.[28] Briefly, this involved a potential step method with a short 1 s pulse at a potential sufficiently negative to reduce the 5-vinyl group of the chromophore to activate bond formation with the catalyst in solution, followed by a 5 s step at a more positive potential. The potential step sequence was repeated for 200 cycles to prepare the fully formed electro-assembled surface. The ALD treatment of the surface did not encumber the electro-assembly of the catalyst layer as evidenced by CV voltammograms before and after the potential step deposition sequence.

The molecular catalyst used here is derived from a family of $[Ru(bda)(L)_2]$ complexes which have been shown as effective catalysts for carrying out the four-electron oxidation of water to O_2.[42,43] In particular, the isoquinoline derivate of this series has demonstrated higher catalytic turnover frequencies as compared with axial pyridine-based complexes.[43,44] Building off our recent work using an axial picoline derivative of the $[Ru(bda)(L)_2]$ catalyst, we pursued the $[Ru(bda)(isoq)_2]$ derivate to take advantage of the higher turnover frequency and thereby reduce

the dwell time of higher valent Ru states of the chromophore or catalyst during photoelectrochemical operation of the cell.

Photoelectrochemical studies of the $[RuP]^{2+}-[Ru(bda)-(isoq)_2]$ electro-assembled surfaces prepared on SnO_2/TiO_2 core−shell substrates showed improved faradaic efficiency for O_2 production in pH 7 as compared with the past system using a $[Ru(bda)(picoline)_2]$ catalyst.[28] Figure 1 shows the result of
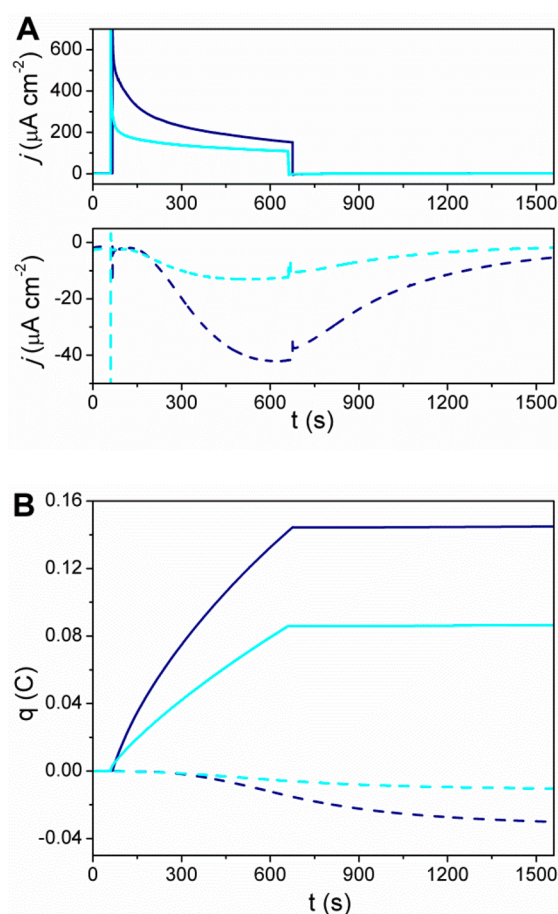

Figure 1. (A) Photocurrent measurement (top frame) taken with an electro-assembled $SnO_2/TiO_2|RuP-Ru(bda)(isoq)_2$ photoanode in pH 7 solution containing 0.1 M phosphate buffer and 0.9 M $NaClO_4$ under an applied bias of 0.4 V vs SCE. The sample was illuminated from 60 to 660 s during the experiment. The dark blue line shows the initial experiment, and the light blue line shows a successive experiment with the same sample taken immediately after the first. The current vs time response at the FTO collector electrode (bottom frame) was measured at −0.85 V vs SCE, and the growth in cathodic current observed from 60 to 660 s results from the reduction of O_2 produced at the photoanode. (B) Charge vs time for the data shown in (A). The faradaic efficiency for the initial experiment was 30% (dark blue) and 17% (light blue) for the following experiment.

photocurrent measurements taken at pH 7 with simultaneous monitoring for photochemically produced O_2 by use of a collector−generator dual working electrode setup.[23] The results of two sequential experiments performed with the same sample are shown. In the first experiment, the high initial photocurrent decays rapidly to around 300 μA cm^{-2} after 200 s and then decays more slowly, reaching a current density of 200 μA cm^{-2} after 10 min of illumination. The photocurrent corresponds to the production of O_2 as measured at the FTO collector electrode. The cathodic current at the collector increases, then

plateaus after ~300 s of illumination, matching the predicted time to reach a steady state flux between two electrodes separated by 1 mm.[23] The stable production of O_2 during the entire 10 min illumination period of the initial experiment contrasts with the electro-assembled surface using the [Ru-(bda)(picoline)$_2$] catalyst, tested under identical conditions, where a decrease in O_2 production was observed after 5 min illumination.

Coinciding with the more stable production of O_2 from water oxidation by this system, the observed faradic efficiency for O_2 production of 30% with the [Ru(bda)(isoq)$_2$] catalyst marks an improvement over the 22% efficiency observed with the [Ru(bda)(picoline)$_2$] derivative at pH 7.[28] In addition, prolonged O_2 production is observed with the faradaic efficiency for a second sequential experiment remaining at 17% whereas effectively no O_2 was observed during a second experiment with the [Ru(bda)(picoline)$_2$] catalyst. The improved performance of the system presented here is most likely a result of improved surface adsorption stability from the ALD overlayer and the use of the more rapid isoquinoline derivative of the [Ru(bda)(L)$_2$] catalyst.

The use of the ALD stabilization overlayer allowed for extending the study of the electro-assembled photoanode to more alkaline conditions. As the chromophore $Ru^{III/II}$ potential is independent of pH, whereas the potential of water oxidation and the potential of the $Ru^{V/IV}$ couple of the catalyst shifts with pH, more overpotential can be supplied by the photo-oxidized chromophore at elevated pH conditions.

The performance of electro-assembled photoanodes at pH 9 is shown in Figure 2. Consistent with past studies, no indication of surface desorption was observed with the ALD stabilized surfaces at this pH.[29] Compared with the performance at pH 7, a modestly higher photocurrent density is observed, though a more pronounced improvement is seen in the faradaic efficiency for O_2 production. The observed efficiency at pH 9 is 45%, representing nearly a 50% increase as compared to the performance at pH 7. This result establishes a promising method for improving overall water splitting efficiencies.

Tandem Photoelectrochemical Water Splitting. Encouraged by the performance of the electro-assembled system on core−shell electrodes, we turned to examining the possibility of carrying out overall water splitting to H_2 and O_2 with only light energy and no applied electrical bias. Since the photoanode uses SnO_2, connecting this photoanode to a platinum cathode would be thermodynamically incapable of driving H_2 formation, as the conduction band of SnO_2 is more positive of the H^+/H_2 formal potential.[45] This in part explains the need for an applied electrical bias when using SnO_2 based photoanodes for DSPEC water splitting applications.[28,34] In place of supplying the needed energy via an electrical bias, we incorporated a second dye-sensitized photovoltaic cell in the circuit to supply a voltage bias to the DSPEC. In this way, light that passes through the photoanode of the DSPEC can be used at the second photocell, with the energy of this second absorbed photon being used to overcome the extra energy needed drive the overall transfer of electrons from the water to H_2.

The development of tandem photochemical systems for carrying out overall water splitting consisting of a semiconductor based photochemical cell wired in series with a DSC have been described elsewhere.[14,15,22] In these studies, direct band gap excitation of a semiconductor initiates the first charge separation event in the system, with the oxidative equivalents driving water oxidation at the semiconductor surface. A PEC using only the
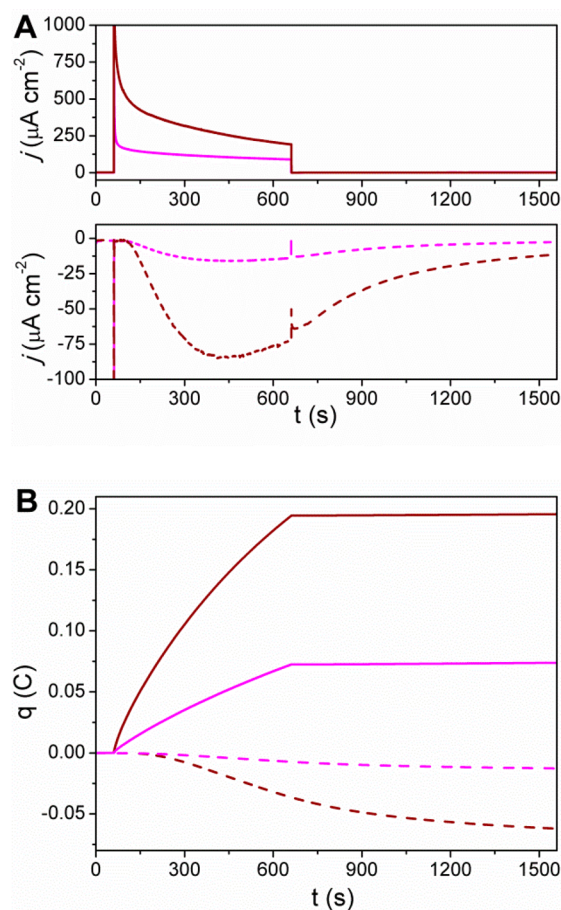

Figure 2. (A) Photocurrent measurement (upper frame) taken with an electro-assembled SnO_2/TiO_2|RuP−Ru(bda)(isoq)$_2$ electrode in pH 9 solution containing 0.1 M phosphate buffer and 0.9 M $NaClO_4$ at an applied bias of 0.4 V vs SCE. The sample was illuminated from 60 to 660 s during the experiment. The dark red line shows the initial experiment, and the magenta line shows a successive experiment with the same sample. The current vs time response of an FTO collector electrode (bottom frame) measured at −0.85 V vs SCE with the growth in cathodic current resulting from the reduction of O_2 generated at the photoanode. (B) Charge vs time for the data shown in (A). The faradaic efficiency for the initial experiment was 45% and 24% for the following experiment.

oxide based photoanode and a dark cathode typically require an applied potential to generate H_2. By connecting a DSC in series, the voltage produced by the DSC under illumination can provide sufficient bias to the PEC such to support spontaneous solar water splitting. As proof of concept, Park and Bard demonstrated a WO_3−DSC system which achieved a solar-to-hydrogen (STH) efficiency of 1.9%.[22] Gratzel, Sivula, and co-workers showed an improved STH of 3.1% using WO_3 with a more optimized DSC component,[14] and Shi et al. have recently achieved an STH of 5.7% with a $WO_3/BiVO_4$ PEC−DSC system.[16]

Recently Sherman et al. described a tandem system incorporating a SnO_2 based DSPEC and TiO_2 based DSC capable of forming hydrogen with hydroquinone used as a sacrificial donor.[18] Due to unfavorable recombination dynamics associated with the use of hydroquinone[46,47] and the more positive conduction band of SnO_2, the DSPEC does not form H_2 without the added energy supplied by the DSC. Here we extend the design of this DSPEC−DSC tandem configuration
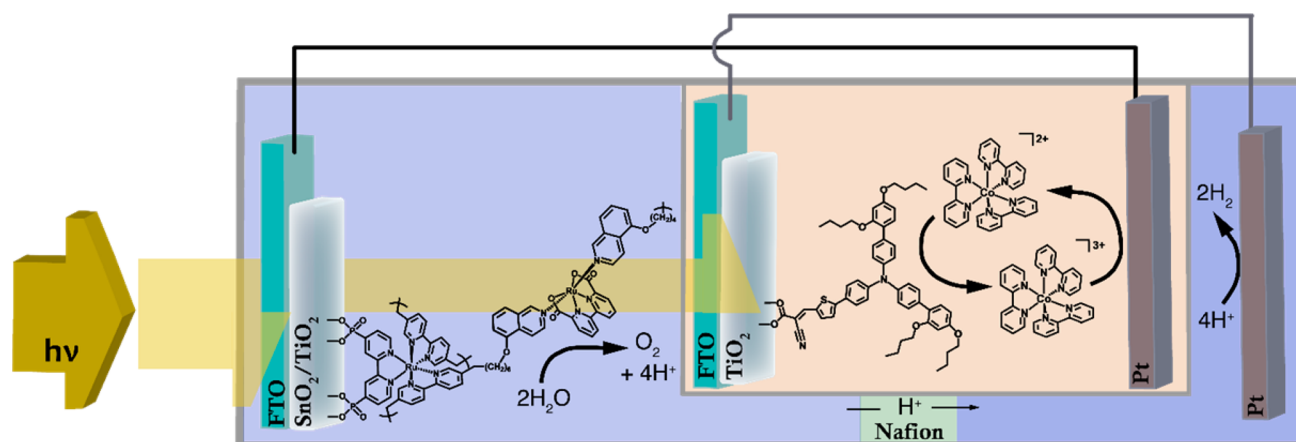
Figure 3. Cell schematic for the electro-assembled core−shell based DSPEC wired in series with DSC D1.

by incorporating a suitable water oxidation catalyst to the DSPEC photoanode to carry out the overall conversion of water to H_2 and O_2 with only light energy and without the need for a sacrificial donor.

The layout of the tandem cell studied here is shown in Figure 3. Light first contacts the photoanode of the DSPEC and then passes to the photoanode of the DSC. Both the DSPEC and DSC utilize a dark cathode, a Pt wire in the case of the DSPEC and platinized FTO in the DSC. The two photochemical cells are connected in series such that the DSPEC photoanode is connected to the FTO−Pt cathode of the DSC, and the DSC photoanode is connected to the Pt wire cathode of the DSPEC by wire leads. The DSPEC and DSC are not otherwise physically connected but are positioned in parallel and perpendicular relative to the light source; that is, the total photon flux through the two photoelectrodes combined is equivalent to 1 sun illumination. They are not independently and simultaneously illuminated at an intensity of 1 sun. The electrolyte solutions in contact with the photoanode and dark cathode of the DSPEC are separated by a Nafion membrane to prevent O_2 or H_2 crossover while maintaining charge balance between the anodic and cathodic chambers.

The fully assembled tandem cell system, depicted in Figure 3, consisted of a DSPEC incorporating a $SnO_2/TiO_2|RuP−Ru(bda)(isoq)_2$ core−shell photoanode, as described in the preceding section, and a Pt cathode wired in series with a DSC. Two different DSCs were explored with N1 employing N719 dye and $I_3^−/I^−$ mediator and D1 using D35 dye and a $[Co(bpy)_3]^{3+/2+}$ mediator.[48] The use of different chromophores gives distinct absorption profiles for each cell. Figure 4 shows a comparison of absorbance spectra for $[RuP]^{2+}$, N719, and D35. The absorbance of both D35 and N719 extend to longer wavelengths as compared to the $[RuP]^{2+}$, with D35 utilizing light out to 550 nm and N719 to 750 nm.

Though the absorbance spectra of D35 and N719 do overlap with that of $[RuP]^{2+}$, this does not prevent either DSC from producing a substantial photocurrent in the tandem configuration. The current vs applied voltage (IV) plots shown in Figure 5 were measured with the DSC placed in the same orientation as in the tandem cell, whereby light first passed through the DSPEC photoanode before illuminating the DSC although the measurements shown in Figure 5 only involve the DSC. Both photocells D1 and N1 still produce substantial short circuit photocurrents, 0.97 mA in the case of D1 and 1.23 mA
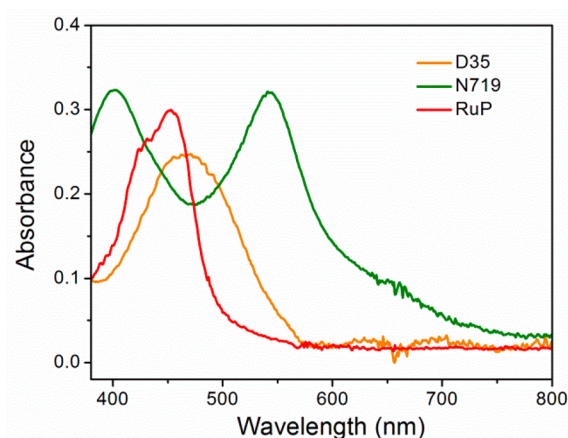

Figure 4. Absorbance spectra for (orange) D35 and (green) N719 recorded in acetonitrile and (red) $[RuP]^{2+}$ recorded in methanol.
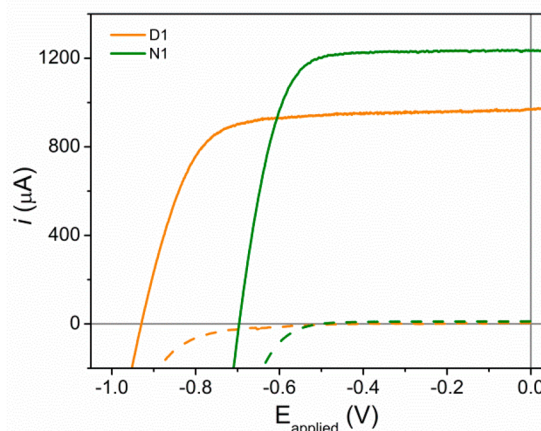

Figure 5. Current vs applied voltage measurements for DSCs D1 (orange, solid) and N1 (green, solid). The dashed lines show the IV response measured under dark conditions. The cells were illuminated with the DSPEC photoanode placed between the cell and the light source to mimic the conditions of the tandem cell though the measurements only involved the DSC. Illumination was supplied by a white light source with an intensity of 100 mW cm^{-2}.

for N1, despite the incident light being obscured by the DSPEC photoanode.

Though producing a lower photocurrent, D1 exhibited a higher open circuit voltage (0.93 V) as compared to N1 (0.7 V). While both DSCs used a TiO$_2$ mesoporous support, the use of different redox mediators, I$_3^-$/I$^-$ for N1 and [Co(bpy)$_3$]$^{3+/2+}$ for D1, produced different open circuit potentials. The potential of the Co$^{III/II}$ couple is reported as 0.57 V vs NHE[27] and I$_3^-$/I$^-$ as 0.35 V vs NHE.[49] The observed difference in open circuit potential (0.23 V) nearly matches the difference in $E_{1/2}$ potentials between the mediators (0.22 V). The ability of the D1 cell to sustain photocurrents at higher applied biases with light that goes unabsorbed at the DSPEC photoanode makes this a better tandem component cell as demonstrated below.

Figure 6 shows a comparison of current vs time plots of the DSPEC with no applied bias (0 V applied between the
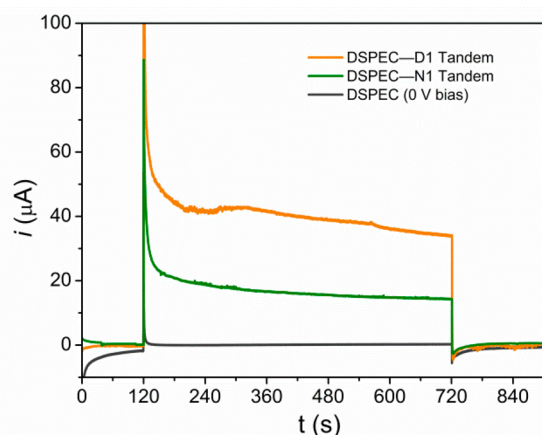

Figure 6. Current vs time plot measured using a DSPEC with a SnO$_2$/TiO$_2$|RuP–Ru(bda)(isoq)$_2$ photoanode (gray) under no applied bias (two electrode configuration) and tandem cells consisting of the same DSPEC wired in series with DSC D1 (orange) and DSC N1 (green). In all measurements, a white light source with an intensity of 100 mW cm^{-2} was used with a 400 nm long pass filter to prevent any direct band gap excitation of the mesoporous semiconductor supports. Each sample was exposed to light from 120 to 720 s during the experiment. The DSPEC photoanode was placed in front of the DSC photoanode such that light first passed through the DSPEC and then contacted the DSC.

photoanode and Pt cathode and no DSC wired in series, gray), the tandem configuration using DSC D1 (orange), and the tandem configuration using DSC N1 (green). For all three experiments, the photocells were illuminated with 100 mW cm^{-2} white light from 120 to 720 s during the experiment. As expected from the open circuit voltage comparison of D1 and N1, the tandem cell produced a higher sustained photocurrent when D1 was placed in series as compared with N1.

As the DSPEC component of the tandem cell is unchanged, the higher photocurrent in the case of the tandem cell with DSC D1 as compared with DSC N1 is due to the intrinsic properties of this photovoltaic cell. As the DSPEC and DSC are wired in series, the total current through the tandem cell will be limited by whichever component sustains a lower photocurrent. Even under substantial applied biases, the DSPEC used here cannot generate photocurrents near, let alone exceed, the ~900 μA produced by D1. In either the case of D1 or N1, current flowing through the tandem cell is not limited by the DSC component. The difference in the observed performance of the tandem cell with D1 or N1 is, however, due to the voltage magnitude either cell can supply to the DSPEC. The photovoltage supplied by the DSC to the DSPEC drives both the collection of charge carriers

at the photoanode back-contact and supplies the needed overpotential at the Pt cathode to generate H$_2$. As seen in Figure 5, D1 generates a 200 mV higher open circuit voltage than N1 and this higher V_{oc} directly correlates to a higher photocurrent observed in the tandem cell.

A direct comparison of the current vs applied voltage plots for the DSPEC and DSC component cells enables a straightforward means of predicting the performance of the tandem cell.[15] Figure 7 shows such a comparison for the system studied here.
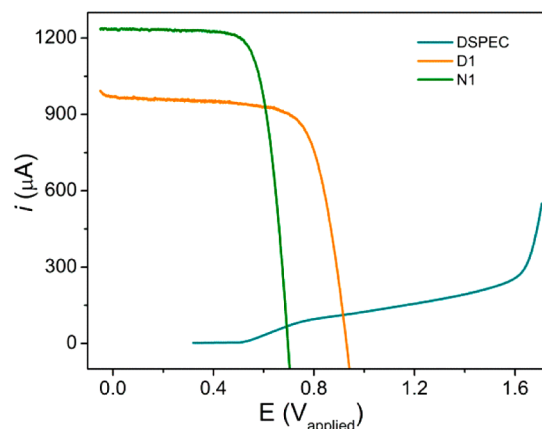

Figure 7. Current vs applied voltage comparison for the DSPEC (blue) and DSC D1 (orange) and N1 (green) under illumination with 100 mW cm^{-2} white light.

In this plot, the applied bias for the DSPEC represents the needed forward bias applied between the DSPEC photoanode and Pt cathode such to sustain current resulting from water oxidation and proton reduction at the respective electrodes. The intersection of the DSC curve with that of the DSPEC represents the predicted operating current of the tandem cell. As visualized here and discussed above, the higher voltage achieved by D1 provides the basis for the improved performance of this tandem cell as compared to that using N1. An additional point illustrated in Figure 7 is that overall lower currents produced by the DSPEC limit the performance of the tandem cell. Improving the DSPEC current magnitude achieved at the voltage intersection between the DSC and DSPEC represents the best means for improving this system.[50]

Figure 8 provides an energy diagram to give perspective of the redox and excited state potentials of the various components comprising the tandem system. The left side of Figure 8 shows the entire tandem cell while the right side shows just the components of the DSC. While the DSCs N1 and D1 utilized different dyes, given the ability of the photoexcited dye to sensitize the TiO$_2$ semiconductor, the open circuit voltage achieved by the DSC will be dictated by the potential difference between the TiO$_2$ conduction band and the redox potential of the mediator species in solution. The [Co(bpy)$_3$]$^{3+/2+}$ mediator couple has a 0.22 V more positive potential compared to I$_3^-$/I$^-$, and this produces the higher magnitude open circuit voltage (as represented by a taller "ΔV"). With the DSC wired in series to the DSPEC, the higher magnitude "ΔV" can generate more overpotential for driving H$_2$ production as represented in the longer downward arrow leading to H$_2$ formation comparing DSPEC–D1 with DSPEC–N1.

Figure 8 illustrates two important considerations for understanding the performance of the DSPEC–DSC tandem architecture. First, while the potential of the DSC components
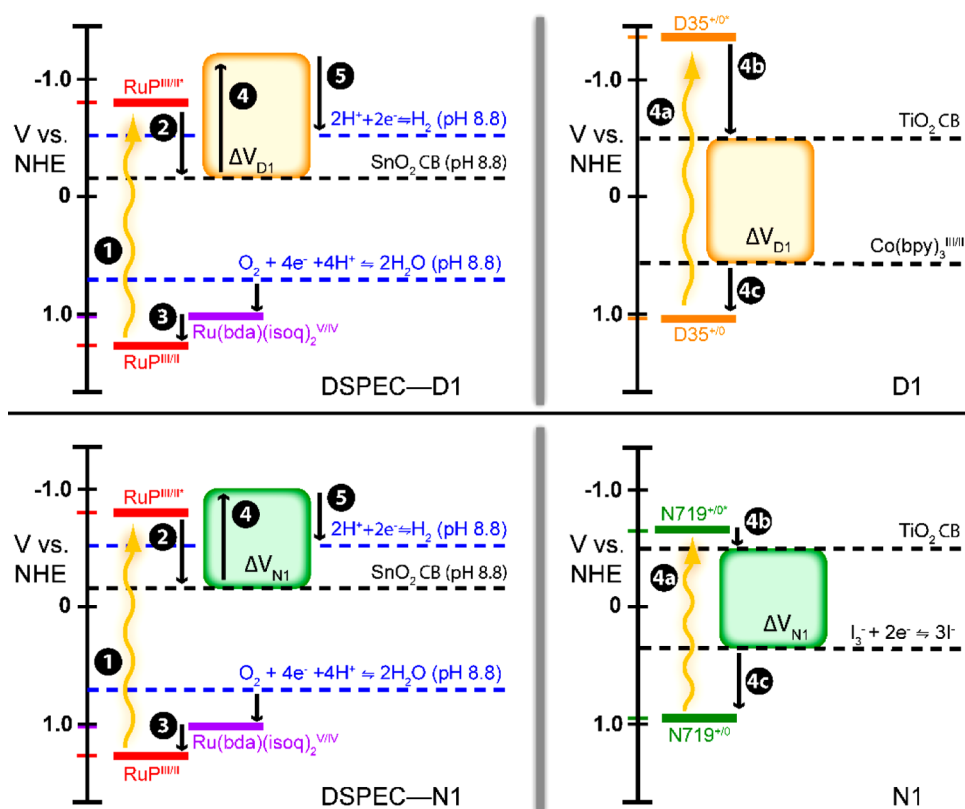
Figure 8. Energy diagram considering the various components of the tandem cell with DSPEC−D1 shown in the top frame and DSPEC−N1 in the bottom frame. The upward arrows represent the increase in potential upon formation of the photoexcited state. Downward arrows represent electron transfer events, and the upward arrow in the box marked "ΔV" indicates the increase in electron energy as supplied by the DSC. The sequential excitation/electron transfer events follow as (1) excitation of the $[RuP]^{2+}$ chromophore; (2) electron injection from the excited state chromophore to the SnO_2/TiO_2 core−shell oxide with the conduction band (CB) potential of SnO_2 indicated; (3) hole transfer from the oxidized chromophore to the $[Ru(bda)(isoq)_2]$ catalyst (four sequential hole transfers are required for each equivalent of O_2 generated, and the potential of the $Ru^{V/IV}$ couple of the catalyst is shown); (4) the photovoltage of the DSC increases the energy of electrons in the circuit with the details of the DSC shown to the right including (4a) excitation of the DSC dye, (4b) electron injection to TiO_2 by the excited state dye, and (4c) hole transfer from the oxidized dye to the reduced form of the mediator (electrons from the DSPEC anode regenerate the reduced form of the mediator at the DSC cathode); and (5) formation of H_2 at the DSPEC cathode.

vs an absolute scale as shown on the right side of Figure 8 are important for understanding the voltage produced by the DSC under illumination, it is only the magnitude of this voltage, and not its placement vs the absolute scale, that matters in considering the operation of the tandem cell (as shown on the left of Figure 8). In the same manner that two identical batteries, with the same anode/cathode chemistries, will generate 2× the voltage of the individual battery when the two are wired in series, the voltage produced by the DSC adds to that of the DSPEC regardless of the absolute level of the TiO_2 conduction band in the DSC. Second, the voltage supplied by the DSC contributes to the flow of current in the tandem cell by providing bias both to collect charge carriers at the FTO−SnO_2 interface and to overcome the needed bias to drive H_2 at the Pt cathode. The conduction band of SnO_2 in pH 8.8 solution is ∼400 mV positive of the thermodynamic potential of hydrogen formation[45] which sets a lower limit for ΔV required from the DSC in order to sustain spontaneous current flow with the tandem cell under illumination.

To verify that the observed photocurrents resulted from the net formation of H_2 from water, for the DSPEC under no applied bias and for the DSPEC−D1 tandem cell, the hydrogen concentration in the headspace over the cathodic chamber of the DSPEC was monitored using an electrochemical probe with a

specific response to H_2 (Unisense, Denmark). The concentration of H_2 in the cathode headspace was monitored simultaneously with the photocurrent measurements shown in Figure 6. As seen in Figures 6 and 9, the DSPEC under no
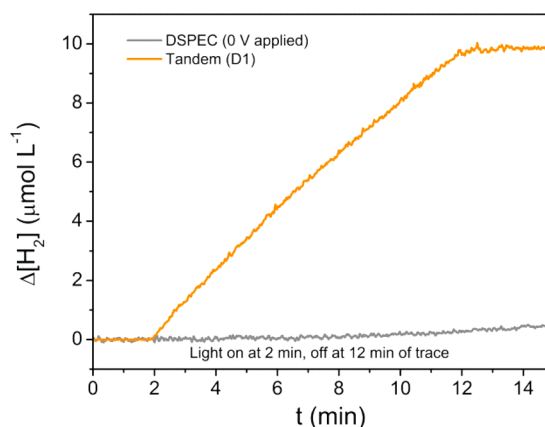

Figure 9. Increase in $[H_2]$ as measured using an electrochemical sensor with specific sensitivity to the presence of H_2. The probe was placed in a sealed chamber housing the Pt cathode which was in ionic contact with the chamber containing the photoanode.

applied bias fails to sustain any photocurrent under prolonged illumination corresponding to no observed net increase in H_2 over the course of the experiment. This observation is consistent with the ubiquitous need for applied bias in DSPEC studies in the literature to sustain a measurable photocurrent density.[28,51−54] It is also consistent with the thermodynamic consequence of using a SnO_2 based photoanode as mentioned above. In the case of the DSPEC−D1 tandem cell, the stable photocurrent corresponds to a steady increase in the amount of hydrogen detected in the sealed headspace of the anodic chamber of the DSPEC.

Measurement of the amount of hydrogen produced during the 10 min illumination period for the top performing DSPEC−D1 tandem cell enables the determination of the solar to hydrogen (STH) efficiency by using eq 1.

$$STH = [(mol\ H_2) \times (2.4 \times 10^5\ J/mol)]$$
$$/[0.1\ W/cm^2 \times A \times t] \tag{1}$$

In eq 1, A is the area of the tandem cell illuminated and t is the duration of the illumination period in seconds. Based on eq 1, an STH efficiency of 0.06% was achieved by the DSPEC−D1 under simulated solar illumination. While this result represents a lower value than that achieved by PEC−DSC systems using the direct band gap excitation of a hematite or tungsten oxide based photoanode,[14−16] it does represent the first instance of a tandem dye-sensitized photoanode based system achieving overall water splitting with the only energy input from simulated solar illumination. The low overall STH is expected from the relatively modest photocurrents (∼40 μA) achieved by the top performing tandem cell. Future work will focus on improving the photocurrents obtained with the DSPEC photoanode.

CONCLUSIONS

This work marks the first use of a dye-sensitized photoanode based tandem photoelectrochemical cell that uses only the energy from solar illumination to convert water to O_2 and H_2. The choice of a DSC as the second photocell component in the system confers certain advantages over other options such as a silicon based PV cell. First, the DSPEC and DSC utilize mesoporous TiO_2 or SnO_2 electrodes which use low-cost and scalable processing techniques for fabrication.[55] Furthermore, DSCs allow for easy modification of both the light absorption characteristics of the cell, through selection and chemical modification of the dye, and the cell voltage achieved under illumination, by tuning the redox potentials of the dye or redox mediator and through selection of semiconductor support. The ability to tune the energetic properties of the photocell is not possible with direct band gap based PV cells (to the extent different band gap materials are available) and could prove an important component in the design of the future devices.

ASSOCIATED CONTENT

ⓢ Supporting Information

The Supporting Information is available free of charge on the ACS Publications website at DOI: 10.1021/jacs.6b10699.

> NMR spectra for 5-(pent-4-en-1-yloxy)isoquinoline and [ruthenium(2,2′-bipyridine-6,6′-dicarboxylic acid)(5-(pent-4-en-1-yloxy)isoquinoline)₂] and electrochemical plots for the electro-assembly of the DSPEC photoanode (PDF)

AUTHOR INFORMATION

Corresponding Author

*tjmeyer@unc.edu

ORCID

Benjamin D. Sherman: 0000-0001-9571-5065

Present Address

†Department of Chemistry, Daegu University, Gyeongsan 38453, Republic of Korea.

Notes

The authors declare no competing financial interest.

REFERENCES

(1) Vitousek, P. M.; Mooney, H. A.; Lubchenco, J.; Melillo, J. M. *Science* **1997**, *277*, 494.

(2) Barnosky, A. D.; Hadly, E. A.; Bascompte, J.; Berlow, E. L.; Brown, J. H.; Fortelius, M.; Getz, W. M.; Harte, J.; Hastings, A.; Marquet, P. A.; Martinez, N. D.; Mooers, A.; Roopnarine, P.; Vermeij, G.; Williams, J. W.; Gillespie, R.; Kitzes, J.; Marshall, C.; Matzke, N.; Mindell, D. P.; Revilla, E.; Smith, A. B. *Nature* **2012**, *486*, 52.

(3) Schramski, J. R.; Gattie, D. K.; Brown, J. H. *Proc. Natl. Acad. Sci. U. S. A.* **2015**, *112*, 9511.

(4) Rockstrom, J.; Steffen, W.; Noone, K.; Persson, A.; Chapin, F. S.; Lambin, E. F.; Lenton, T. M.; Scheffer, M.; Folke, C.; Schellnhuber, H. J.; Nykvist, B.; de Wit, C. A.; Hughes, T.; van, d. L.; Rodhe, H.; Sorlin, S.; Snyder, P. K.; Costanza, R.; Svedin, U.; Falkenmark, M.; Karlberg, L.; Corell, R. W.; Fabry, V. J.; Hansen, J.; Walker, B.; Liverman, D.; Richardson, K.; Crutzen, P.; Foley, J. A. *Nature* **2009**, *461*, 472.

(5) Sherman, B. D.; Vaughn, M.; Bergkamp, J. J.; Gust, D.; Moore, A. L.; Moore, T. A. *Photosynth. Res.* **2014**, *120*, 59.

(6) Bard, A. J.; Fox, M. A. *Acc. Chem. Res.* **1995**, *28*, 141.

(7) Concepcion, J. J.; House, R. L.; Papanikolas, J. M.; Meyer, T. J. *Proc. Natl. Acad. Sci. U. S. A.* **2012**, *109*, 15560.

(8) Blankenship, R. E. *Molecular Mechanisms of Photosynthesis*; Wiley-Blackwell: Oxford, 2002.

(9) Bolton, J. R.; Strickler, S. J.; Connolly, J. S. *Nature* **1985**, *316*, 495.

(10) Hanna, M. C.; Nozik, A. J. *J. Appl. Phys.* **2006**, *100*, 074510.

(11) Blankenship, R. E.; Tiede, D. M.; Barber, J.; Brudvig, G. W.; Fleming, G.; Ghirardi, M.; Gunner, M. R.; Junge, W.; Kramer, D. M.; Melis, A.; Moore, T. A.; Moser, C. C.; Nocera, D. G.; Nozik, A. J.; Ort, D. R.; Parson, W. W.; Prince, R. C.; Sayre, R. T. *Science* **2011**, *332*, 805.

(12) Khaselev, O.; Turner, J. A. *Science* **1998**, *280*, 425.

(13) Licht, S.; Wang, B.; Mukerji, S.; Soga, T.; Umeno, M.; Tributsch, H. *J. Phys. Chem. B* **2000**, *104*, 8920.

(14) Brillet, J.; Yum, J. H.; Cornuz, M.; Hisatomi, T.; Solarska, R.; Augustynski, J.; Graetzel, M.; Sivula, K. *Nat. Photonics* **2012**, *6*, 824.

(15) Prevot, M. S.; Sivula, K. *J. Phys. Chem. C* **2013**, *117*, 17879.

(16) Shi, X.; Zhang, K.; Shin, K.; Ma, M.; Kwon, J.; Choi, I. T.; Kim, J. K.; Kim, H. K.; Wang, D. H.; Park, J. H. *Nano Energy* **2015**, *13*, 182.

(17) Li, F.; Fan, K.; Xu, B.; Gabrielsson, E.; Daniel, Q.; Li, L.; Sun, L. *J. Am. Chem. Soc.* **2015**, *137*, 9153.

(18) Sherman, B. D.; Bergkamp, J. J.; Brown, C. L.; Moore, A. L.; Gust, D.; Moore, T. A. *Energy Environ. Sci.* **2016**, *9*, 1812.

(19) Odobel, F.; Le Pleux, L. c.; Pellegrin, Y.; Blart, E. *Acc. Chem. Res.* **2010**, *43*, 1063.

(20) Yella, A.; Lee, H.; Tsao, H. N.; Yi, C.; Chandiran, A. K.; Nazeeruddin, M. K.; Diau, E. W.; Yeh, C.; Zakeeruddin, S. M.; Grätzel, M. *Science* **2011**, *334*, 629.

(21) Brillet, J.; Cornuz, M.; Formal, F. L.; Yum, J.; Grätzel, M.; Sivula, K. *J. Mater. Res.* **2010**, *25*, 17.

(22) Park, J. H.; Bard, A. J. *Electrochem. Solid-State Lett.* **2006**, *9*, E5.

(23) Sherman, B. D.; Sheridan, M. V.; Dares, C. J.; Meyer, T. J. *Anal. Chem.* **2016**, *88*, 7076.

(24) Ashford, D. L.; Sherman, B. D.; Binstead, R. A.; Templeton, J. L.; Meyer, T. J. *Angew. Chem.* **2015**, *127*, 4860.

(25) Li, F.; Zhang, B.; Li, X.; Jiang, Y.; Chen, L.; Li, Y.; Sun, L. *Angew. Chem., Int. Ed.* **2011**, *50*, 12276.

(26) Hagberg, D. P.; Jiang, X.; Gabrielsson, E.; Linder, M.; Marinado, T.; Brinck, T.; Hagfeldt, A.; Sun, L. *J. Mater. Chem.* **2009**, *19*, 7232–7238.

(27) Koh, T. M.; Nonomura, K.; Mathews, N.; Hagfeldt, A.; Gratzel, M.; Mhaisalkar, S. G.; Grimsdale, A. C. *J. Phys. Chem. C* **2013**, *117*, 15515.

(28) Sherman, B. D.; Ashford, D. L.; Lapides, A. M.; Sheridan, M. V.; Wee, K. R.; Meyer, T. J. *J. Phys. Chem. Lett.* **2015**, *6*, 3213.

(29) Lapides, A. M.; Sherman, B. D.; Brennaman, K.; Dares, C. J.; Skinner, K. R.; Templeton, J.; Meyer, T. J. *Chem. Sci.* **2015**, *6*, 6398.

(30) Ito, S.; Murakami, T. N.; Comte, P.; Liska, P.; Grätzel, C.; Nazeeruddin, M. K.; Grätzel, M. *Thin Solid Films* **2008**, *516*, 4613.

(31) Abruna, H. D. *Coord. Chem. Rev.* **1988**, *86*, 135.

(32) Ashford, D. L.; Lapides, A. M.; Vannucci, A. K.; Hanson, K.; Torelli, D. A.; Harrison, D. P.; Templeton, J. L.; Meyer, T. J. *J. Am. Chem. Soc.* **2014**, *136*, 6578.

(33) Zhong, Y.; Yao, C.; Nie, H. *Coord. Chem. Rev.* **2013**, *257*, 1357.

(34) Alibabaei, L.; Sherman, B. D.; Norris, M. R.; Brennaman, M. K.; Meyer, T. J. *Proc. Natl. Acad. Sci. U. S. A.* **2015**, *112*, 5899.

(35) Knauf, R. R.; Kalanyan, B.; Parsons, G. N.; Dempsey, J. L. *J. Phys. Chem. C* **2015**, *119*, 28353.

(36) Karlsson, M.; Jõgi, I.; Eriksson, S. K.; Rensmo, H. k.; Boman, M.; Boschloo, G.; Hagfeldt, A. *Chimia* **2013**, *67*, 142.

(37) Ghosh, P. K.; Brunschwig, B. S.; Chou, M.; Creutz, C.; Sutin, N. *J. Am. Chem. Soc.* **1984**, *106*, 4772.

(38) Limburg, B.; Bouwman, E.; Bonnet, S. *Coord. Chem. Rev.* **2012**, *256*, 1451.

(39) Roecker, L.; Kutner, W.; Gilbert, J. A.; Simmons, M.; Murray, R. W.; Meyer, T. J. *Inorg. Chem.* **1985**, *24*, 3784.

(40) Hyde, J. T.; Hanson, K.; Vannucci, A. K.; Lapides, A. M.; Alibabaei, L.; Norris, M. R.; Meyer, T. J.; Harrison, D. P. *ACS Appl. Mater. Interfaces* **2015**, *7*, 9554–9562.

(41) Hanson, K.; Losego, M. D.; Kalanyan, B.; Parsons, G. N.; Meyer, T. J. *Nano Lett.* **2013**, *13*, 4802.

(42) Duan, L.; Fischer, A.; Xu, Y.; Sun, L. *J. Am. Chem. Soc.* **2009**, *131*, 10397.

(43) Duan, L.; Bozoglian, F.; Mandal, S.; Stewart, B.; Privalov, T.; Llobet, A.; Sun, L. *Nat. Chem.* **2012**, *4*, 418.

(44) Song, N.; Concepcion, J. J.; Binstead, R. A.; Rudd, J. A.; Vannucci, A. K.; Dares, C. J.; Coggins, M. K.; Meyer, T. J. *Proc. Natl. Acad. Sci. U. S. A.* **2015**, *112*, 4935–4940.

(45) Hagfeldt, A.; Graetzel, M. *Chem. Rev.* **1995**, *95*, 49.

(46) Hambourger, M.; Liddell, P. A.; Gust, D.; Moore, A. L.; Moore, T. A. *Photochem. Photobiol. Sci.* **2007**, *6*, 431.

(47) Hambourger, M.; Kodis, G.; Vaughn, M. D.; Moore, G. F.; Gust, D.; Moore, A. L.; Moore, T. A. *Dalton Trans.* **2009**, 9979.

(48) Feldt, S. M.; Gibson, E. A.; Gabrielsson, E.; Sun, L.; Boschloo, G.; Hagfeldt, A. *J. Am. Chem. Soc.* **2010**, *132*, 16714.

(49) Boschloo, G.; Hagfeldt, A. *Acc. Chem. Res.* **2009**, *42*, 1819.

(50) Sheridan, M. V.; Sherman, B. D.; Coppo, R. L.; Wang, D.; Marquard, S. L.; Wee, K. R.; Murakami Iha, N. Y.; Meyer, T. J. *ACS Energy Lett.* **2016**, *1*, 231.

(51) Youngblood, W. J.; Lee, S. H. A.; Kobayashi, Y.; Hernandez-Pagan, E. A.; Hoertz, P. G.; Moore, T. A.; Moore, A. L.; Gust, D.; Mallouk, T. E. *J. Am. Chem. Soc.* **2009**, *131*, 926.

(52) Moore, G. F.; Blakemore, J. D.; Milot, R. L.; Hull, J. F.; Song, H.; Cai, L.; Schmuttenmaer, C. A.; Crabtree, R. H.; Brudvig, G. W. *Energy Environ. Sci.* **2011**, *4*, 2389.

(53) Zhao, Y.; Swierk, J. R.; Megiatto, J. D.; Sherman, B.; Youngblood, W. J.; Qin, D.; Lentz, D. M.; Moore, A. L.; Moore, T. A.; Gust, D.; Mallouk, T. E. *Proc. Natl. Acad. Sci. U. S. A.* **2012**, *109*, 15612.

(54) Gao, Y.; Ding, X.; Liu, J.; Wang, L.; Lu, Z.; Li, L.; Sun, L. *J. Am. Chem. Soc.* **2013**, *135*, 4219–4222.

(55) Gratzel, M. *Nature* **2001**, *414*, 338.